Design and Fabrication of a 1 THz Backward Wave Amplifier

Paoloni, Claudio; Di Carlo, Aldo; Brunetti, Francesca; Mineo, Mauro; Ulisse, Giacomo; Durand, Alain; Krozer, Viktor; Kotiranta, Mikko; Fiorello, Anna Maria; Dispenza, Massimiliano

Total number of authors:
18

Published in:
Terahertz Science & Technology

Publication date:
2011

Document Version
Publisher's PDF, also known as Version of record

Invited Paper

Design and Fabrication of a 1 THz Backward Wave Amplifier

Claudio Paoloni [1*], Aldo Di Carlo [1°], Francesca Brunetti [1], Mauro Mineo [1], Giacomo Ulisse [1], Alain Durand [2], Viktor Krozer [3], Mikko Kotiranta [3], Anna Maria Fiorello [4], Massimiliano Dispenza [4], Alberto Secchi [4], Vitaly Zhurbenko [5], Faycal Bouamrane [6], Thomas Bouvet [6], Stephan Megtert [6], Emanuela Tamburri [7], Costel-Sorin Cojocaru [8], Aurelien Gohier [8]

[1] Dept. of Electronic Engineering, University of Rome Tor Vergata, Via del Politecnico 1, 00133, Rome, Italy
[*] Email: claudio.paoloni@uniroma2.it

[°] OPTHER project coordinator: aldo.dicarlo@uniroma2.it

[2] Thales Electron Devices, Vélizy, France

[3] Physikalisches Institut, Goethe-Universität Frankfurt am Main, Frankfurt am Main, Germany

[4] Selex-SI, Rome, Italy

[5] Technical University of Denmark, Kgs. Lyngby, Denmark

[6] Unité Mixte de Physique CNRS-THALES et Université Paris sud 11, Palaiseau, France

[7] Dept. of Chemical Science and Technology, University of Rome Tor Vergata, Rome, Italy

[8] LPICM – École Polytechnique, (UMR 7647) CNRS, Palaiseau, France

(Received September 16, 2011)

Abstract: The THz frequency range represents a true challenge for designers, fabrication technologies and characterization systems. So far, huge technological obstacles have prohibited any system realization different from laboratory one. Furthermore, most of the applications in the THz frequency range require a level of power not achievable by optoelectronic devices at room temperature or by solid-state technology. The recent availability of three-dimensional simulators and high aspect ratio micro-fabrication techniques has stimulated a class of vacuum electron devices operating in the THz regime, to get a level of output power to enable applications at these frequencies. The OPTHER (Optically driven THz amplifier) project, funded by the European Community, is on the road to realize the first 1 THz vacuum tube amplifier. Technology at the state of the art has been used for the realization of the parts with dimensions supporting THz frequencies. A backward wave amplifier configuration is chosen to make the parts realizable. A carbon nanotube cold cathode has been considered for electron generation. A thermionic micro electron gun is designed to test the tube. A novel slow-wave structure (SWS), the double corrugated rectangular waveguide, is devised to support a cylindrical electron beam and to guarantee high interaction impedance with limited losses. Both LIGA and UV SU-8 photolithography have been tested to realize the SWS.

Keywords: Terahertz, Carbon nanotube, Micromachining, LIGA, Vacuum electron device, Backward wave amplifier

1. Introduction

A new frontier has been opened in the field of vacuum electron devices in the THz frequency range (100-1500 *GHz*), by the introduction of MEMS technology, cold cathodes, and high-aspect ratio photolithographic fabrication process [1-3]. The opportunity of reducing the dimensions of vacuum tubes to the micrometric range has fed the prospective of enabling a wide number of applications at THz frequencies [4-6] that require power levels at room temperature which are currently unattainable, in a compact and affordable way. Many research groups are active

worldwide in the task of realizing vacuum electron devices, both amplifiers and oscillators for THz applications [7-22].

THz vacuum electron devices remain in the state-of-the-art field. Simulation and fabrication represent a true challenge requiring innovative approaches to be won.

Simulation requires high accuracy models and procedures valid at THz frequencies. Due to relatively new interest in the THz regime, a relevant effort of characterization and theoretical studies are still in progress to improve the simulator accuracy. Metal losses at THz frequencies are a key issue, in particular their dependence on the surface roughness [7], [23]. The introduction of unconventional shapes of THz interaction structures requires highly flexible three-dimensional electromagnetic simulators. Particle-in-cell simulators are required to evaluate the interaction of the RF field with the electron beam and the overall tube performance. Due to the three dimensional nature of these simulators, the computation task is formidable and time consuming.

Fabrication is strongly influenced by the micrometric dimensions of the parts. Four different phases can be individuated: realization of electromagnetic parts, realization of a cathode and an electron gun, assembling and vacuum pumping. All of them are critical and stress the fabrication process. Parts with dimensions in the range of tens of microns, to support the interaction of the electron beam with the THz RF field, can be realized only by recent micromachining, MEMS or photolithographic techniques. Among them, the most affordable are surely Direct Ion Etching (DRIE) and UV SU-8 photolithography [2], but X-ray LIGA (German acronym of lithography, electroplating, and molding) [7] assures the highest aspect ratio and the smallest relative dimensions. Micro electron guns, whether thermionic or cold cathode [24] ones, are required to generate a high quality electron beam with the desired current. Carbon nanotubes (CNTs) are deeply investigated as electron emitters in cold cathode [25-28]. The assembling, due to the tight tolerances in the micron range, requires a proper design of the parts to minimize effects due to imperfections and misaligning. High vacuum pumping of submillimeter vacuum electron devices is a very difficult task. In order to avoid ion collisions and other problems related to a poor vacuum level, which are particularly critical in a tube with micrometric dimensions, the tube design has to be adjusted to get the best possible vacuum level as well.

The OPTHER (Optically driven THz amplifier) project, funded by the European Community, has faced all these challenges with the objective of realizing the first vacuum tube amplifier in THz frequency range. The main specifications are 10 *dB* gain at 1 *THz*, low weight, small dimensions (1 dm^3) and a beam voltage lower than 12 *kV* for portability. The constraint on the maximum allowed beam voltage (12*kV*) at the given operating frequency makes it very hard to fabricate a slow-wave structure (SWS) in forward wave regime, due to the dimensions too small. In particular, the required SWS period length at 1 *THz* is currently unattainable in a reliable way with the available fabrication processes. On the contrary, the backward wave regime [29-31], based on the synchronism of the electron velocity with the phase velocity of the first backward harmonic (n = -1), permits to overcome this limitation. For a given SWS, the same frequency can be obtained with a much lower beam voltage than in forward wave regime or, for the same beam voltage, a longer SWS period can be used. Differently to the forward-wave regime, the electron velocity is opposite to the group velocity, so a backward wave amplifier (BWA) presents the input port on the collector side and the output port on the gun side. The backward-wave amplifier topology was adopted to design and realize the OPTHER amplifier. The intrinsic narrow band

characteristic of the BWA is compatible with the specifications of the OPTHER project.

In the following, the main aspects related to the microfabrication of the parts of the 1 *THz* BWA amplifier are outlined. The SWS is described in Section 2. Section 3 discusses the approach to the micro electron gun. The approach to the design of input and output couplers and the related fabrication technology are presented in Section 4 and finally simulation results on the backward wave amplifier at 1 *THz* are reported in Section 5.

2. Slow-wave structure

Rectangular corrugated waveguides [32-35] are particularly suitable as THz slow-wave structures due to the compatibility with high aspect-ratio photolithographic processes. A conventional corrugated waveguide, due to the distribution of the *z*-component of the electric field on the top of the corrugation, interacts effectively with a sheet beam. Currently, magnetic focusing and gun designs for a sheet beam are at a research level [36], so the use of a cylindrical beam was preferred as a safer solution. To overcome the limited interaction region between a cylindrical beam and a rectangular corrugated waveguide, an innovative solution was adopted: the double corrugated waveguide (Fig. 1) [37]. The novel SWS effectively supports a cylindrical beam, maintaining the fabrication characteristics of a corrugated waveguide. From the fabrication point of view, the corrugations and the lateral walls can be realized in a single step and the top plane in a second step. The assembling is highly reliable, since possible sealing residuals allocated between the sidewalls and the top cover or misalignment do not significantly affect the electric field distribution, concentrated around the corrugation and located far from the sidewalls. The hollow nature of the SWS is particularly suitable for an effective vacuum pumping.

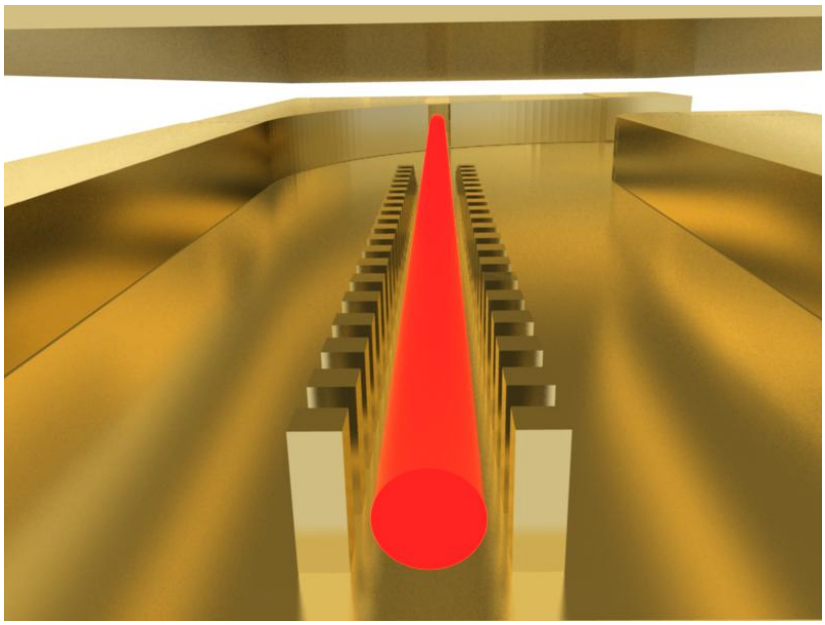

Fig. 1 Rendering of the double corrugated waveguide with a beam and a detached top plane

In case of a beam voltage lower than 12 *kV*, a period in the order of 40-50 μm is required in the backward wave regime. Such a period is fully compatible with the features of photolithographic

processes.

A double corrugated rectangular waveguide was designed to work at the operating frequency of about 1 *THz* and with a 10 *kV* beam voltage (Fig. 2). The cold parameters for the backward wave region computed by a 3-D electromagnetic simulator (CST-MWS) [38] are shown in Fig. 3. The 10 *kV* beam line intercepting the dispersion curve is shown as well. The material of the simulated structure was copper, the conductivity of which was decreased based on the information obtained by extrapolating the results of low frequency loss measurements. The computed losses are moderate, about 0.15 *dB/cell*, while interaction impedance is 2 *Ω*, at the operating frequency.

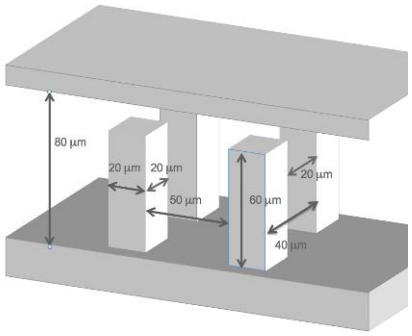

Fig. 2 Dimensions of the designed double corrugated waveguide (1*THz* frequency and 10 *kV* beam voltage in backward wave regime)

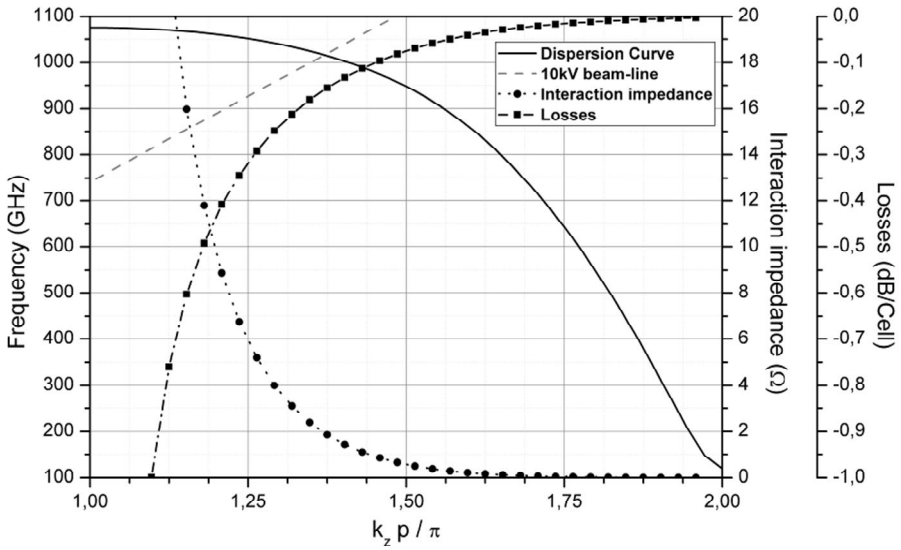

Fig. 3 Dispersion, interaction impedance and losses for the double corrugated waveguide in backward wave regime.

3. Electron beam generation

When the dimensions of the interaction structure are in the order of tens of microns, the dimensions of the electron beam have to be defined accordingly. In addition, the level of losses at THz frequencies could be very high, requiring a relatively high beam current. This can be achieved with a cathode having a high current density or a wide emission area. The first option is

more suitable for thermionic cathodes. The second option has to be adopted when using cold cathodes [24], carbon nanotube cathodes in particular, which at the moment do not provide high current densities [25-27]. Both approaches are valid for electron gun realization and worth of consideration. For OPTHER project, as previously written, a cylindrical electron beam has been chosen to limit the focusing issues and to enable the use of the well-established Pierce gun technology. A beam radius of 20 μm is the design target.

A thermionic electron gun which requires complex manufacturing techniques, has to include a heater, but presents limited electrostatic focusing problems and assures the required beam radius and current.

An electron gun based on CNT cold cathode is a new challenging approach to beam generation that would be very suitable for THz vacuum devices, since it allows one not only to obtain a compact, room temperature and durable apparatus, but also to preliminary pattern the beam shape. The CNT cathode is realized by growing the CNTs on purposely patterned substrate using chemical vapor deposition (CVD) techniques. Differently from thermionic electron gun, in case of a CNT cold cathode, the emission is prone to the transverse electron velocity that has to be carefully controlled and limited. The particle-in-cell (PIC) simulations (MAGIC3D) [39] of an electron beam affected (a) and not affected (b) by transverse electron velocity are shown in Fig. 4. The design of the CNT cold cathode is focused to minimize this phenomenon maintaining the highest current density [28].

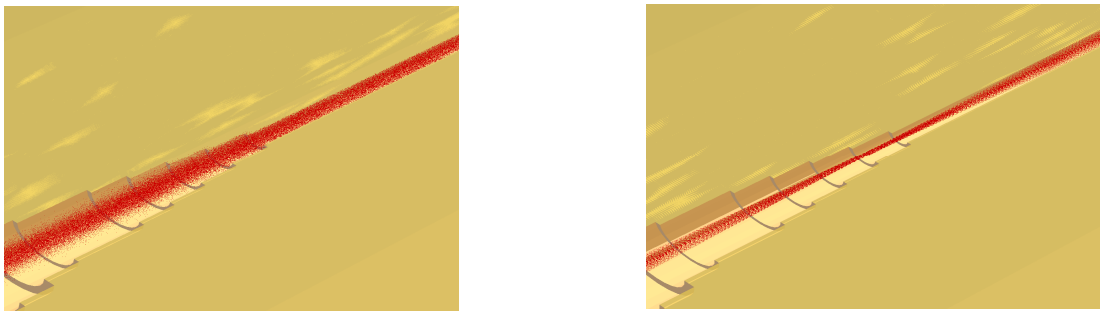

(a) (b)

Fig. 4 Effect of transverse velocity on the focusing: an electron beam propagating in the electron gun anode (a) without transverse velocity, (b) with transverse velocity

Two different configurations of the cathode, the external grid cathode (Fig. 5(a)) and the integrated grid cathode (Fig. 5(b)), were designed, simulated and realized for the purpose.

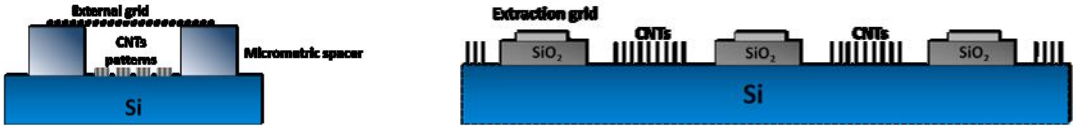

(a) (b)

Fig. 5 External grid (a) and integrated-grid (b) cathode

In the first case, an external grid separated from the cathode with an insulating mechanical

spacer has been adopted. The cathode-grid distance is in the order of few tens of microns. Nanometric (Fig. 6(a)) and micrometric (Fig. 6(b)) patterns of carbon nanotubes were realized by different synthesis method. Unfortunately, in this case the transverse velocity of the electrons is of about 10 *eV*, provoking a current loss of more than 80% of the total emitted current at the anode. For the realized samples, the maximum emitted current density measured, calculated on the emitting areas, is 0.15 A/cm^2.

The integrated grid cathode consists of an array of micrometric square patterns of emitters and an integrated extraction grid. A single element of the array has an emitting area containing vertically aligned nanotubes with a height of 1 μm. After the optimization of the structure in terms distance of the grid from the CNTs and the height of the CNTs, a minimum transverse velocity of 63 *meV* was obtained for the simulated devices. The CNTs were grown on a silicon/silicon oxide substrate. The technological process is based on four different phases: realization of the aperture (oxide etching); deposition of the metal grid (first alignment, grid sputtering and lift-off); definition of the pattern for the growth of carbon nanotubes (second alignment, metal catalyst deposition and lift-off); growth of carbon nanotubes. An example of the realized samples, which provides a current density of about 74 mA/cm^2 with a maximum applied extracting voltage of 80 *V*, is shown in Fig. 6(c). A study on the behavior of the current density as a function of the extracting voltage demonstrates that a much higher current density can be obtained by increasing the voltage. Technological efforts are currently devoted to realize an extracting grid able to support voltage higher than 80 *V*.

The goal is to obtain performance not far from the one of a thermionic cathode. This will permit the use of a very light and compact electron gun based on a CNT cold cathode.

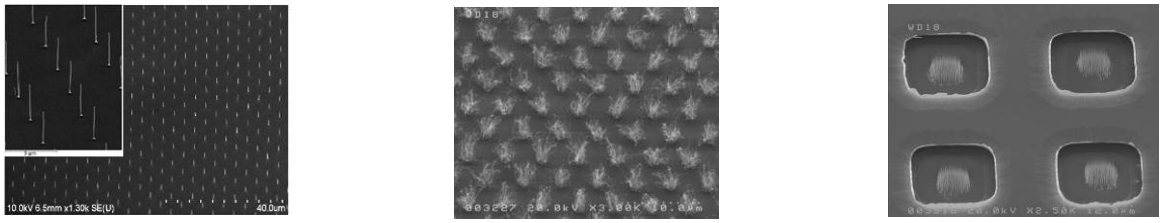

(a) (b) (c)

Fig. 6 (a) nanometric pattern, (b) micrometric pattern, (c) integrated grid array

4. Input and output coupling and fabrication of the parts

Once the dimensions and the number of periods of the SWS are defined, input and output couplers are required. The practical implementation of the slow-wave structure requires a design of an efficient RF excitation scheme, which is a challenging problem in the considered frequency range. The excitation part of the structure must be fabricated in the same technological process as the slow-wave structure in order to avoid alignment problems.

Due to the short wavelength at THz frequencies, the physical dimensions of the SWS excitation structure are inherently small. This imposes severe constraints on the fabrication process error tolerance. Current microfabrication technologies are restricted to 2D patterning. Adding features and varying geometries in the third dimension (height) using a layer-by-layer

approach is theoretically appealing but very difficult in practice, because alignment problems often lead to fabrication errors comparable with the feature size of the structure.

Another possibility to shape the structure in different dimensions is to turn it around with regard to the exposure direction, but this moves the problem to the post processing of the structure. Moving, and especially rotating, a miniature structure is very tricky. Moreover, the slow-wave structure along with the excitation part of it should finally be aligned with the precision of a few microns on the distance of several millimeters or even centimeters in order to allow for unobstructed electron-beam propagation in the device.

Another challenge is associated with increasing attenuation of an electromagnetic signal in the THz range. This imposes a significant additional constraint on the size of the excitation structure. The size should be as small as possible in terms of the electromagnetic wave propagation path in order to minimize the losses in the excitation region. On the other hand, the requirement for broadband operation leads to long SWS excitation structures in terms of wavelengths. This trade-off between the insertion loss and bandwidth requires a careful analysis and leads to an extensive optimization of the excitation structure profile.

A problem of a slow-wave mode excitation concerns a transformation of the fundamental mode of an external guiding structure, such as a rectangular waveguide, into an operating mode of the slow-wave structure. Different types of slow-wave structures have different field distributions and therefore usually require specific excitation schemes. Nevertheless, a universal method for the design of an excitation structure can be implemented in our case, which is based on tapering of the slow-wave structure parameters. These parameters are associated with the physical dimensions of the structure. For the structure considered in this work, the double corrugated slow-wave structure, the tapering of the corrugation height, corrugation width and the distance between two corrugations have been considered. The considered structures are shown in Fig.7(a), (b) and (c) with top cover removed. An alternative approach to the slow-wave excitation is to use a short-circuited stub for the reflected wave compensation, as shown in Fig.7(d).

The height-tapering configuration in Fig. 7(a) exhibits the best matching properties among all configurations, but it is difficult to realize using a photolithographic process. Stub matching in Fig. 7(d) is also excluded, because it also requires complex fabrication processes. The tapering of the distance between the two corrugations (Fig.7(c)) has been chosen for the realization of the excitation structure.

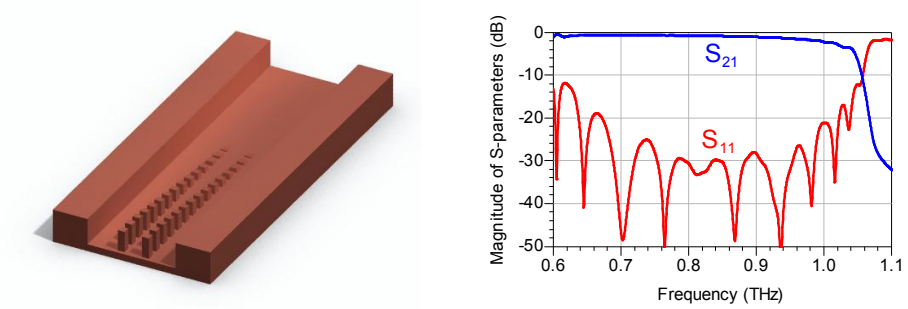

(a)

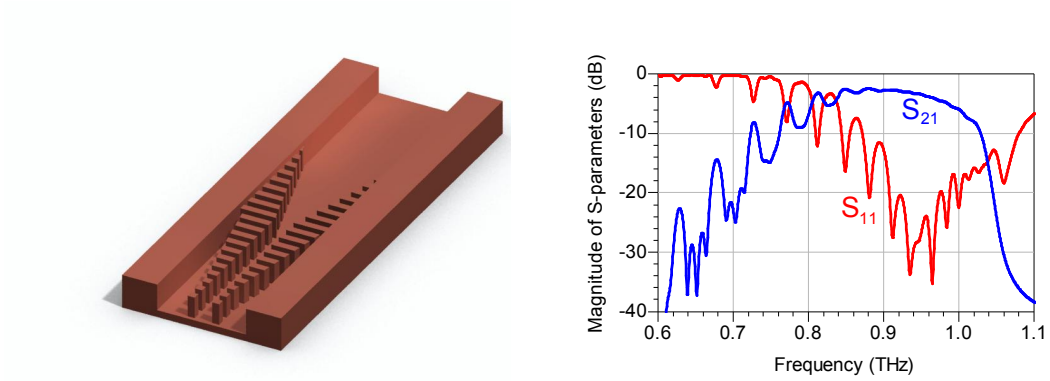

(b)

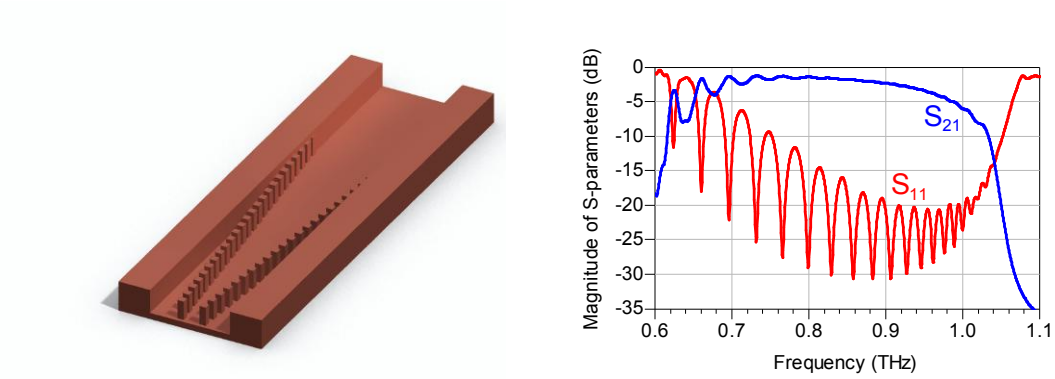

(c)

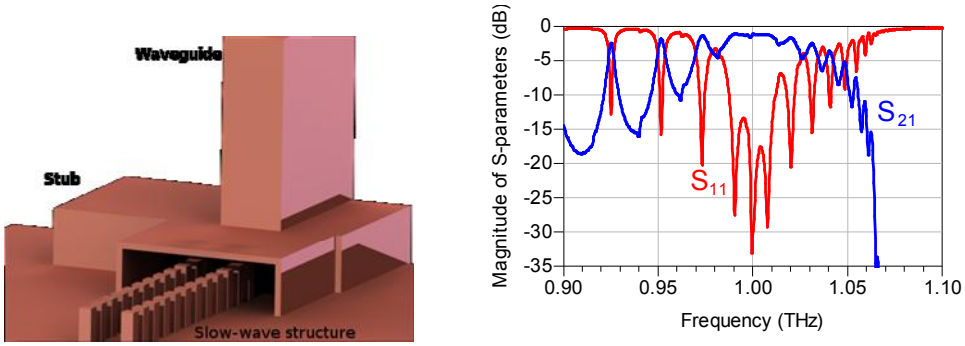

(d)

Fig. 7 Schematic and scattering parameters of different input/output coupler types in back-to-back configuration: (a) height tapering; (b) corrugation width tapering; (c) corrugation distance tapering; (d) stub matching.

To evaluate the effect of the couplers on a possible BWA layout, the S-parameters of a structure based on lateral tapering couplers and 10 periods of double corrugated waveguide Fig.8(b) are computed by frequency domain electromagnetic simulator (CST-MWS). The tapers at the input and output ends are followed by a 90-degree waveguide bend. The outer sidewall of each bend has an opening to a drifting channel of the electron beam. In this arrangement, the feeding waveguide is perpendicular to the slow-wave structure, and the power can be fed away from the entrance path of the electron beam. The size of the rectangular waveguide is 254 μm ×

80 μm. The total insertion loss at 1 THz is approximately 10 *dB* Fig. 8(b). The frequency band where the return loss is better than 15 *dB* is from 0.86 *THz* to 1.015 *THz*. The upper cut-off frequency is related to the dispersion characteristic of the slow-wave structure itself.

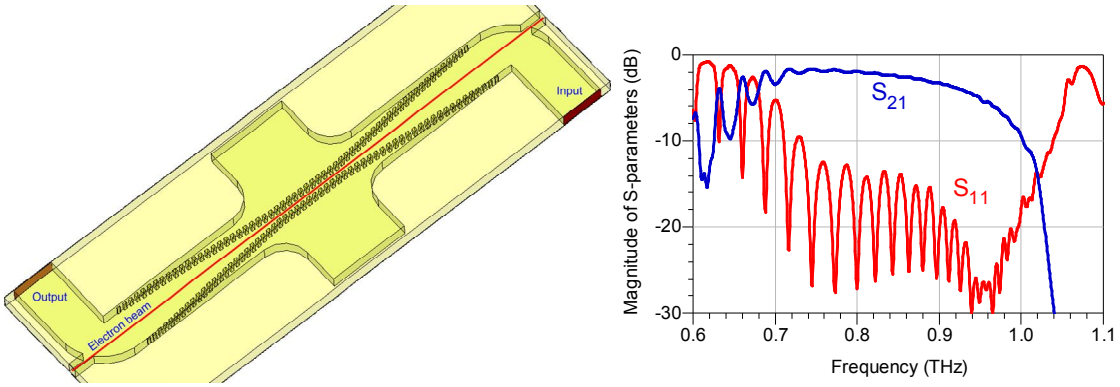

(a) (b)

Fig. 8 (a) Structure with the input and output couplers and 10 SWS periods, (b) the simulated S-parameters.

A photograph of the realized double corrugated structure with tapered distance of the corrugations and with the top cover removed is shown in Fig. 9. The fabrication was achieved by means of DXRL (Deep X-Ray Lithography) technology, which is able to handle the requested high precision (both dimension and position). First the PMMA (poly (methyl methacrylate)) resist was casted at room temperature.

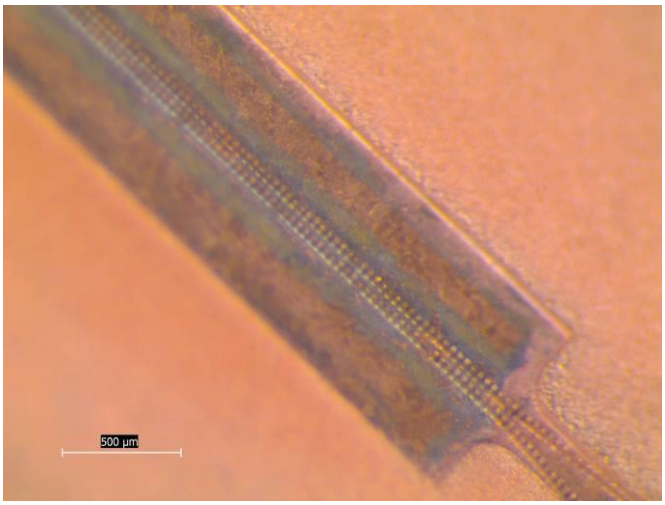

Fig. 9 Overview of the double corrugated waveguide and couplers realized with X-ray LIGA process.

After a polishing step to bring the PMMA to the required thickness (80-100 μm), flatness and parallelism, it was covered with 0.1-0.2 μm thick evaporated gold (plating base) layer, and then a 25 μm thick SU-8 layer was spun coated on top. A standard chromium mask was used, which guarantee an accuracy of better than 0.1 μm for the dimensions and relative positions of the structures. The duplication of the chromium mask to manufacture a DXRL mask maintains the precision of the structure dimensions and their relative positioning within the tolerance of 1μm. A special substrate holder was designed to perform the positioning of the chromium mask relative to the set of HCOF (High Conductivity Oxygen Free) copper substrates (precision required was

+/-2 μm). After development, gold was electroplated up to a thickness of 15-20 μm.

The PMMA resist, covered by the self-supported mask, was exposed to synchrotron light at SOLEIL, on the LIGA station set up on Metrology beam line. The used radiation dose at the bottom of the resist was calculated to be 3 kJ/cm^3. The substrate was kept at 20°C during the exposure in order to avoid heating of the PMMA and the mask on top due to the absorbed high photon flux. After the exposure, the PMMA was then developed with a standard developer for 2-3 *hours* and rinsed in de-ionized water for 10 *minutes*. The PMMA realization of the coupler and a detail of the double corrugated waveguide are shown in Fig. 10. Afterwards copper (acidic base) was electroplated at room temperature up to a thickness of 70 μm for the SWS and up to 30 μm for the cover.

In order to gently remove the remaining PMMA a new exposure was done using the LIGA station followed by the last development. The detail of the double corrugated waveguide, with a teeth height of 60 μm, is clearly visible, as well as the coupler, at the upper left corner of Fig. 11. The distance between adjacent corrugations increases linearly from 50 μm to 254 μm within 25 *periods* of the slow-wave structure until the corrugations merge with the walls of the rectangular waveguide.

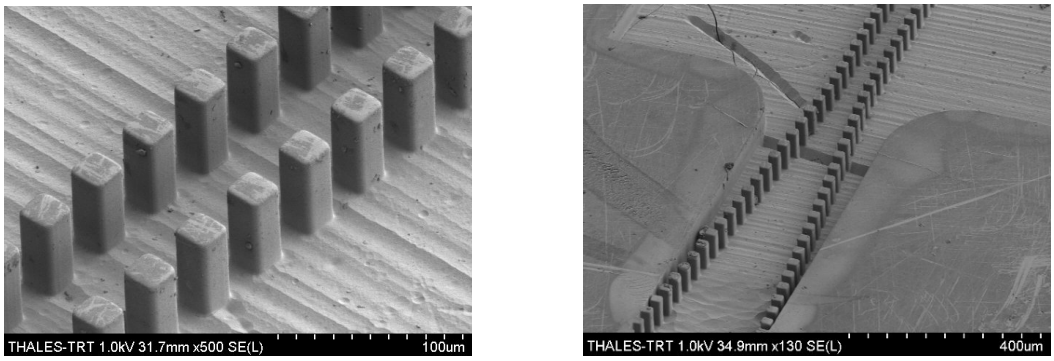

(a) (b)

Fig. 10 PMMA realization (a) coupler and double corrugated waveguide, (b) detail of the corrugations (mold with negative tone).

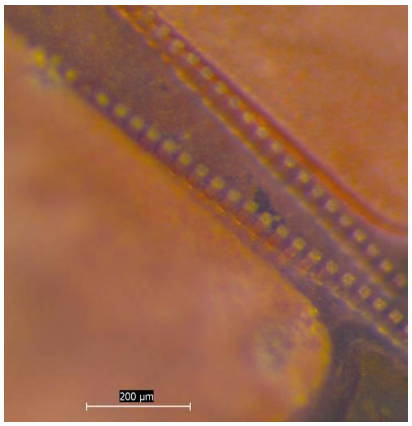

Fig. 11 Detail of the copper realization of the double corrugated waveguide coupler fabricated with X-ray LIGA process.

A parallel effort is in progress to implement the same structure by using more standard and lower cost UV photolithography, based on high-resolution photoresists such as SU-8, KMPR and similar others. The technological process is based on a negative photoresist definition followed by gold electroplating. Patterns with wide clear areas in the mask impose a severe limitation to aspect ratios due to the large amount of UV light scattering. This makes the fabrication of isolated pillars more challenging than patterning periodic combs with the same aspect ratio. Very good results were obtained for regular corrugated periodic structures (teeth up to 70 μm high, and 20 μm wide) as shown in Fig. 12(a). The manufactured double corrugation waveguide and the coupler did not yet satisfy the design requirements due to the height of corrugations under 40 μm (Fig. 12(b)), but improvement of the fabrication process is ongoing.

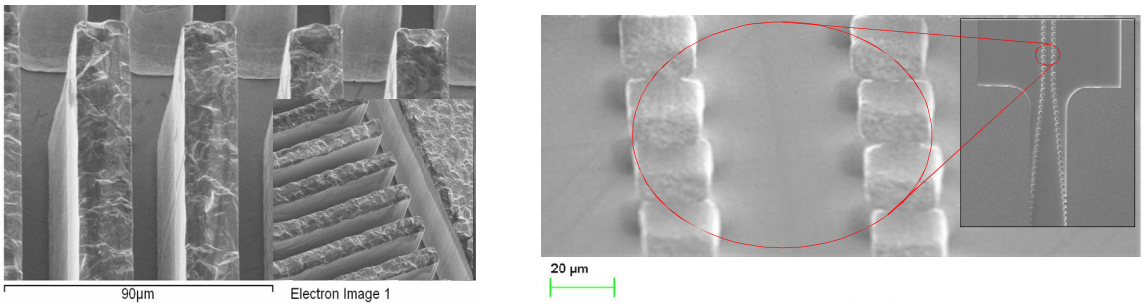

(a) (b)

Fig. 12 Two SWSs realized by SU-8 based UV photolithography: (a) regular corrugated periodic structure; (b) double corrugated waveguide and coupler (isolated pillars).

5. Backward wave amplifier simulation

The successful fabrication of the interaction structures and of the other parts demonstrates feasible the design of a 1 *THz* backward wave amplifier.

The double corrugated waveguide in Fig. 2 was used as SWS for a central operating frequency of 1 *THz* and 10 *kV* of beam voltage. A cylindrical electron beam with a radius of 20 μm was chosen and aligned with a 5 μm distance from the corrugation walls. A magnetic focusing field of 0.8 *T* was applied to assure the proper beam confinement. The number of periods was 155. To limit the complexity of the simulation the electron gun was replaced by an emitting surface with radius equal to the beam radius were used.

The first step of the BWA design is to evaluate the starting current of oscillation for the given beam voltage, current and number of periods of the SWS. The evaluation was carried out by a first series of three-dimension particle-in-cell (PIC) simulations (MAGIC3D) [39]. A starting current for oscillation of 6.0 *mA* was obtained. Once the starting current is known, a beam current slightly lower is chosen, 5.0 *mA* in this case. Then, the BWA performance was evaluated by a 3-D PIC simulation. An input signal of 100 μW at 1 *THz* was injected in the input port. The electron energy as a function of the *z*-coordinate is shown in Fig. 13 (a). The power spectrum of the input and output signal at central operating frequency are shown in Fig. 13(b). A gain of about 12 *dB* is obtained. The PIC simulation required about 500 *hours* of computer time.

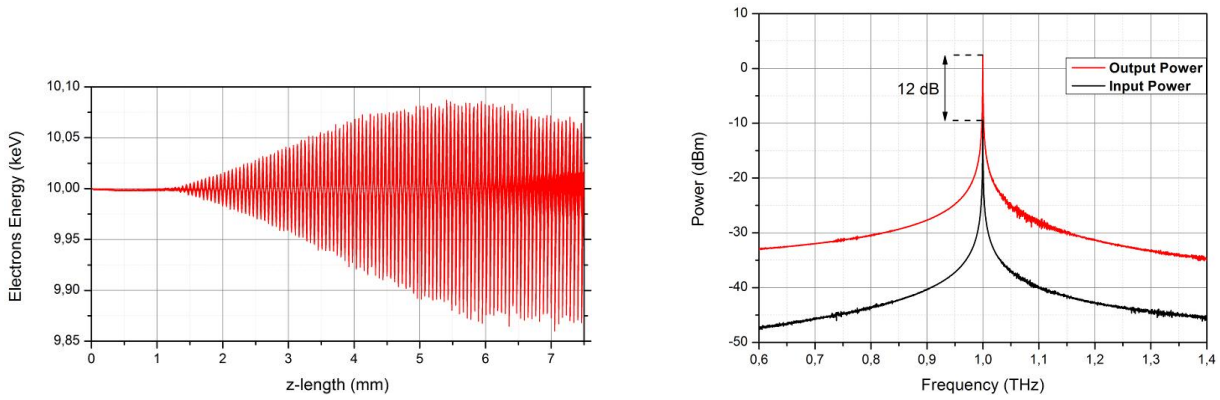

(a) (b)

Fig. 13 (a) Electron energy as a function of the SWS length (b) Output and input power spectrum

Finally, the different parts will be assembled in a sealed envelope. The rendering of a possible solution for the final assembling of the 1 *THz* BWA is shown in Fig. 14. The compact structure includes the gun, the collector and the SWS encapsulated in an envelope.

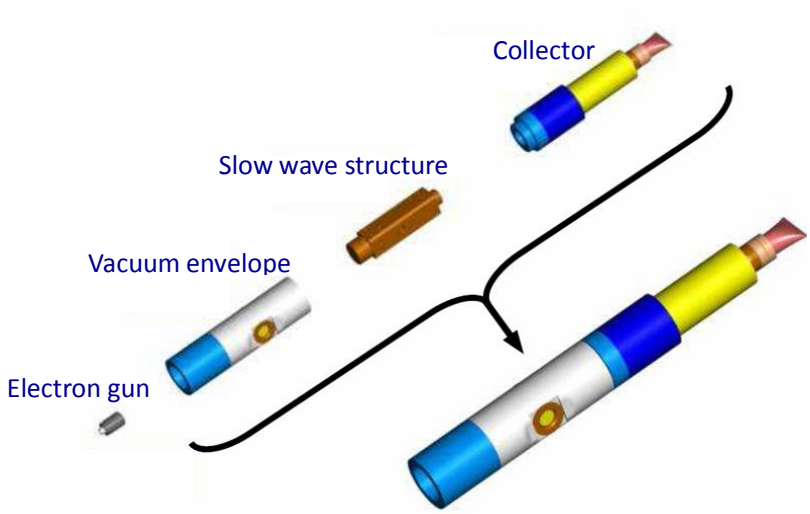

Fig. 14 Rendering of the preliminary assembling of the 1-*THz* backward wave amplifier.

6. Conclusions

The design and fabrication of a state-of-the-art 1*THz* vacuum backward wave amplifier, in the frame of the OPTHER project, are currently on going. The different design and fabrication steps have been described, highlighting the state of the art solution adopted for a successful result. The adoption of the backward wave regime, high aspect-ratio fabrication processes and innovative solutions for the SWS and the couplers have been demonstrated as the most effective way to realize a 1 *THz* BWA.

Acknowledgment：

This work has been supported by the FP-7 European Project No. 224356 “OPTHER- Optically Driven THz Amplifiers”.

The authors would like to thank Mourad Idir, Pascal Mercère and Paulo Da Silva from the Laboratoire SOLEIL (Saint-Aubin, France) for dedicated beam time allocated to this project and Silvia Orlanducci for the fruitful discussion on the CNTs synthesis.

References

[1] R. L. Ives, “Microfabrication of High-Frequency Vacuum Electron Devices”， *IEEE Trans. On Plasma Science*, 32, 3, 1277-1291, (2004).

[2] R. A. Lawes, “Manufacturing tolerances for UV LIGA using SU-8resist”, *Journal of Micromechanics and Microengineering*, 15, 2198-2203(6), (2005).

[3] Y. M. Shin, L. R. Barnett, and N. C. Luhmann, Jr., "Terahertz vacuum electronic circuits fabricated by UV lithographic molding and deep reactive ion etching", *Appl. Phys. Lett.* 95, 181505, (2009).

[4] J. F. Federici, B. Schulkin, F. Huang, D. Gary, R. Barat, F. Oliveira, and D. Zimdars, “THz imaging and sensing for security applications - explosives, weapons and drugs”, *Semiconductor Science and Technology*, 20, 7, 266-280, (2005).

[5] P.H.Siegel, “Terahertz Technology”, *IEEE Trans. on Microwave Theory and Techniques*, 50, 3, 910-928, (2002).

[6] C. Sirtori, “Applied Physics: Bridge for the terahertz gap”, *Nature*, 417, 9, 132–133, (2002).

[7] Y. M. Shin, J. K. So, S. T. Han, K. H. Jang, G. S. Park, J. -Hyun Kim and Suk-Sang Chang, "Microfabrication of millimeter wave vacuum electron devices by two-step deep-etch x-ray lithography", *Appl. Phys. Lett*. 88, 091916 (2006).

[8] Y. M. Shin, L. R. Barnett, and N. C. Luhmann, Jr., “Phase-Shifted Traveling-Wave-Tube Circuit for Ultrawideband High-Power Submillimeter-Wave Generation”, *IEEE Trans. on Electron Devices*, 56, 5, 706-712, (2009).

[9] L. Earley, B. Carlsten, F. Krawczyk, J. Potter, F. Sigler, E. Smirnova, R. Wheat, C. Heath and A. Bailey, “Wideband RF Structure for Millimeter Wave TWTs”, *AIP Conf. Proc*. 807 335 (2006)

[10] G. P. Scheitrum, “Microfabricated MVEDs” in *Modern Microwave and Millimeter Wave Power Electronics*, Eds. Piscataway, NJ: IEEE Press, 343-391, (2005).

[11] A. Korolev, S. Zaitsev, I. Golenitskij, Y. Zhary, A. Zakurdayev, M. Lopin, P. Meleshkevich, E. Gelvich, A. Negirev, A. Pobedonostsev, V. Poognin, V. Homich, and A. Kargin, "Traditional and novel vacuum electron devices", *IEEE Trans. On Electron Devices*, 48, 12, 2929-2937, (2001).

[12] Y. M. Shin, L. R. Barnett, and N. C. Luhmann, Jr., “Strongly confined plasmonic wave propagation through an ultrawideband staggered double grating waveguide”, *Appl. Phys. Lett.* 93, 221504 (2008).

[13] C. Kory, L. Ives, M. Read, J. Booske, H. Jiang, D. van der Weide, and P. Phillips, “Microfabricated W-band traveling wave tubes”, *Proc. Infrared Millimeter Waves/13th Int. Conf. Terahertz Electron,* 1, 85-86, (2005).

[14] S. -T. Han, S. -G. Jeon, Y. -M. Shin, K. -H. Jang, and J. -K. So, J. -H. Kim, S. -S. Chang, and G. -S. Park, "Experimental investigations on miniaturized high-frequency vacuum electron devices", *IEEE Trans. on Plasma Science*, 33, 2, 679–684, (2005).

[15] S. Bhattacharjee, J. H. Booske, C. L. Kory, D. W. van der Weide, S. Limbach, S. Gallagher, D. Welter, M. R. Lopez, R. M. Gilgenbach, R. L. Ives, M. E. Read, R. Divan, and D. C. Mancini, "Folded waveguide traveling-wave tube sources for terahertz radiation", *IEEE Trans. Plasma Science*, 32, 3, 1002-1014, (2004).

[16] R. Zheng, P. Ohlckers, and X. Chen, "Particle-in-Cell Simulation and Optimization for a 220-GHz Folded-Waveguide Traveling-Wave Tube", *IEEE Trans. on Electron Devices,* 58, 7, 2164-2171, (2011).

[17] Y. M. Shin, A. Baig, L. R. Barnett, N. C. Luhmann, Jr., J. Pasour, and P. Larsen, "Modeling Investigation of an Ultrawideband Terahertz Sheet Beam Traveling-Wave Tube Amplifier Circuit", *IEEE Trans. on Electron Devices,* 58, 9, 3213-3218, (2011).

[18] X. Xu, Y. Wei, F. Shen, Z. Duan, Y. Gong, H. Yin, W. Wang, "Sine Waveguide for 0.22THz Traveling Wave Tube", IEEE Electron Devices Letters, 32, 8, 1152-1154, (2011).

[19] R. Dobbs, R. Roitman, P. Horoyskia, M. Hyttinen, D. Sweeney, B. Steer, K. Nguyen, E. Wright, D. Chernin, A. Burke, J. Calame, B. Levush, N. S. Barkere J. Booske, M. Blank, "Design and fabrication of terahertz extended interaction klystrons", *35th IRMMW-THz Conference*, 1-3, (2010).

[20] J. Tucek, D. Gallagher, K. Kreischer, and R. Mihailovich, "A compact, high power, 0.65 THz source", *IEEE International Vacuum Electronics Conference Proceedings*, *(IVEC 2008),* 16-17, (2008).

[21] M. Mineo, C. Paoloni, "Corrugated Rectangular Waveguide Tunable Backward Wave Oscillator for Terahertz Applications", *IEEE Trans. on Electron Devices,* 57, 6, 1481-1484, (2010).

[22] M. Kotiranta, V. Krozer, V. Zhurbenko, "Square Helix TWT for THz Frequencies", *35th IRMMW-THz Conference*, 1-2, (2010).

[23] S. Lucyszyn and Y. Zhou, "Engineering Approach to Modelling Metal THz Structures", Terahertz Science and Technology, 4, 1, (2011).

[24] D. R. Whaley, R. Duggal, C. M. Armstrong, C. L. Bellew, C. E. Holland, and C. A. Spindt, "100 W Operation of a Cold Cathode TWT", *IEEE Trans. on Electron Devices,* 56, 5, 896-905, (2009).

[25] L. Silan, D. L. Niemann, B. P. Ribaya, M. Rahman, M. Meyyappan and C. V. Nguyen, "Novel Geometry of Carbon Nanotube Field Emitter to Achieve High Current Densities for Terahertz Sources", *IEEE International Vacuum Electronics Conference Proceedings*, *(IVEC 2009),* 16-17, (2009).

[26] P. Legagneux, N. Le Sech, P. Guiset, L. Gangloff, C. Cojocaru, J. P. Schnell, D. Pribat, K. B. K. Teo, J. Robertson, W. I. Milne, F. Andre, Y. Rozier, D. Dieumegard, "Carbon nanotube based cathodes for microwave amplifiers", *IEEE International Vacuum Electronics Conference Proceedings, (IVEC 2009) ,* 80-81, (2009)

[27] F. André, P. Ponard, Y. Rozier, C. Bourat, L. Gangloff, S. Xavier, "TWT and X-Ray Devices Based on Carbon Nano-Tubes", *IEEE International Vacuum Electronics Conference Proceedings, (IVEC 2010),* 83-84, (2010).

[28] G. Ulisse, F. Brunetti, A. Di Carlo, "Study of the Influence of Transverse Velocity on the Design of Cold Cathode-Based Electron Guns for Terahertz Devices", *IEEE Trans. on Electron Devices,* 58, 9, 3002-3004, (2011).

[29] H. Heffner, "Analysis of the Backward-Wave Traveling-Wave Tube", *Proceedings of the IRE*, 42, 6, 930-937, (1954).

[30] R. Kompfner and N. T. Williams, "Backward Wave Tubes", *Proceedings of the IRE*, 41, 11, 1602-16011, (1953).

[31] J. Gewartowski and H. Watson, Principles of Electron Tubes. NJ: Van Nostrand, (1965).

[32] B. McVey, M. Basten, J. Booske, J. Joe, and J. Scharer, "Analysis of rectangular waveguide-gratings for amplifier applications*", IEEE Trans. on Microwave Theory and Techniques*, 42, 6, 995-1003, (1994).

[33] G. Zaginaylov, A. Hirata, T. Ueda, and T. Shiozawa, "Full-wave modal analysis of the rectangular waveguide grating", *IEEE Transactions on Plasma Science*, 28, 3, 614-620, (2000).

[34] M. Mineo, C. Paoloni, A. Di Carlo, A. M. Fiorello, M. Dispenza, "Corrugated waveguide slow-wave structure for THz traveling wave tube", *Proc. European Microwave Conference, 2009*, 842-845, (2009).

[35] J. Joe, J. Scharer, J. Booske and B. McVey, "Wave dispersion and growth analysis of low-voltage grating Čerenkov amplifiers", *Physics of Plasmas*, 1, 1, 176-188, (1994).

[36] K. T. Nguyen, J. A. Pasour, T. M. Antonsen, P. B. Larsen, J. J. Petillo; B. Levush, "Intense Sheet Electron Beam Transport in a Uniform Solenoidal Magnetic Field", *IEEE Trans. On Electron Devices*, 56, 5, 744-752, (2009)

[37] M. Mineo, C. Paoloni, "Double-Corrugated Rectangular Waveguide Slow-Wave Structure for Terahertz Vacuum Devices", *IEEE Trans. on Electron Devices,* 57, 11, 3169-3175, (2010).

[38] [Online]. Available: www.cst.com

[39] B. Goplen, L. Ludeking, D. Smithe, and G. Warren, "User-configurable MAGIC for electromagnetic PIC calculations", *Comput. Phys. Commun.* 87, 1/2, 54-86, (1995).